Depolarization-activated gating pore current conducted by mutant sodium channels in potassium-sensitive normokalemic periodic paralysis

Stanislav Sokolov, Todd Scheuer, and William A. Catterall[1]

Department of Pharmacology, University of Washington, Seattle, WA 98195-7280

Contributed by William A. Catterall, October 20, 2008 (sent for review September 25, 2008)

Some inherited periodic paralyses are caused by mutations in skeletal muscle $Na_V1.4$ sodium channels that alter channel gating and impair action potential generation. In the case of hypokalemic periodic paralysis, mutations of one of the outermost two gating charges in the S4 voltage sensor in domain II of the $Na_V1.4$ α subunit induce gating pore current, resulting in a leak of sodium or protons through the voltage sensor that causes depolarization, sodium overload, and contractile failure correlated with low serum potassium. Potassium-sensitive normokalemic periodic paralysis (NormoPP) is caused by mutations in the third gating charge in domain II of the $Na_V1.4$ channel. Here, we report that these mutations in rat $Na_V1.4$ (R669Q/G/W) cause gating pore current that is activated by depolarization and therefore is conducted in the activated state of the voltage sensor. In addition, we find that this gating pore current is retained in the slow-inactivated state and is deactivated only at hyperpolarized membrane potentials. Gating pore current through the mutant voltage sensor of slow-inactivated NormoPP channels would cause increased sodium influx at the resting membrane potential and during trains of action potentials, depolarize muscle fibers, and lead to contractile failure and cellular pathology in NormoPP.

skeletal muscle | Na_v 1.4 | gating charge | voltage sensor

Voltage-gated sodium channels in skeletal muscle ($Na_V1.4$) generate action potentials that initiate muscle contraction in response to nerve stimulation. They are complexes of a large pore-forming α-subunit and a small, auxiliary $\beta1$-subunit (1–4). The α-subunits are organized in 4 repeated domains with 6 transmembrane segments (S1–S6) and a reentrant P loop between S5 and S6 (4, 5). The voltage sensitivity of sodium channels arises from the force of the transmembrane electric field exerted on arginine residues in 3-residue repeat motifs in the S4 transmembrane segments, which move outward upon depolarization and initiate a conformational change that opens the central pore (4, 6).

The periodic paralyses are rare, dominantly inherited muscle disorders characterized by episodic attacks of muscle weakness (7). Hyperkalemic periodic paralysis (HyperPP) and paramyotonia congenita are caused by mutations in the α subunit of skeletal muscle $Na_V1.4$ channels that are widely spread through the protein and usually cause a gain-of-function by impairing fast and/or slow inactivation (8). Increased sodium channel activity leads to depolarization, hyperexcitability, and either repetitive firing or depolarization block. In contrast, hypokalemic periodic paralysis (HypoPP) is caused by mutations in both the α-subunit of the $Na_V1.4$ channel and the homologous $\alpha1$-subunit of the skeletal muscle $Ca_V1.1$ channel, which initiates excitation–contraction coupling (8). In HypoPP, mutations in both of these large channel proteins specifically target the outermost two gating-charge-carrying arginine residues in their S4 voltage sensors in domains II, III, or IV. The convergence of these mutations on the outermost two gating charges of voltage sensors in two different proteins strongly implicates voltage sensor dysfunction in this disease. Standard electrophysiological studies of these mutant sodium channels expressed in heterologous cells revealed only mildly enhanced fast and/or slow inactivation (9–12), but more sensitive recordings in the cut-open oocyte preparation showed that HypoPP mutant $Na_V1.4$ channels conduct gating pore currents caused by movement of protons and cations through the mutant voltage sensor (13, 14). Gating pore current constitutes a gain-of-function effect because steady influx of cations at resting membrane potential would cause depolarization and sodium overload that impair action potential generation.

HypoPP is diagnosed by episodic weakness during low serum potassium, whereas HyperPP is diagnosed by initiation of episodes of weakness by administration of potassium. Some patients with periodic paralysis have serum potassium in the normal physiological range during attacks of weakness (3.0–5.5 mM) (15–17), suggesting an intermediate category of normokalemic periodic paralysis (NormoPP). However, studies of patients with the T704M mutation revealed increased blood potassium levels during attacks in 50% of cases (18), and some of families diagnosed as NormoPP were subsequently found to have the HyperPP mutations T704M or M1592V, leading to the suggestion that NormoPP may be a phenotypic variant of HyperPP (19). In contrast to those studies, Vicart *et al.* (20) reported 4 families with unique mutations, leading to 3 different substitutions for the R3 gating charge in domain II of the $Na_V1.4$ channel, R675G/Q/W, for human $Na_v1.4$. Serum potassium levels during attacks were normal (3.0–5.5 mM) in 5 patients. However, some of the patients also experienced severe attacks of weakness with decreased serum potassium, similar to the HypoPP phenotype, whereas others had attacks induced by a potassium supplement as in HyperPP. Here, we use the abbreviation NormoPP to refer specifically to potassium-sensitive normokalemic periodic paralysis caused by mutations in the R3 gating charge, as reported by Vicart *et al.* (20).

Mutations of the outer two gating charges in the S4 segment of domain II of brain $Na_V1.2$ channels cause gating pore current in the resting state, whereas mutation of the third gating charge causes gating pore current in the activated state (21). Because gating pore current is unique to voltage sensors and is a gain-of-function effect, we tested NormoPP mutants in rat $Na_v1.4$ for gating pore current. We report here that all three NormoPP mutants conduct substantial gating pore currents that are activated by depolarization. Moreover, these mutant channels conduct gating pore current in both activated and slow-inactivated states, which would cause increased influx of sodium near the resting membrane potential, membrane depolarization, sodium overload, action potential failure, and cellular pathology in NormoPP.

Author contributions: S.S., T.S., and W.A.C. designed research, performed research, analyzed data, and wrote the paper.

The authors declare no conflict of interest.

[1]To whom correspondence should be addressed. E-mail: wcatt@u.washington.edu.

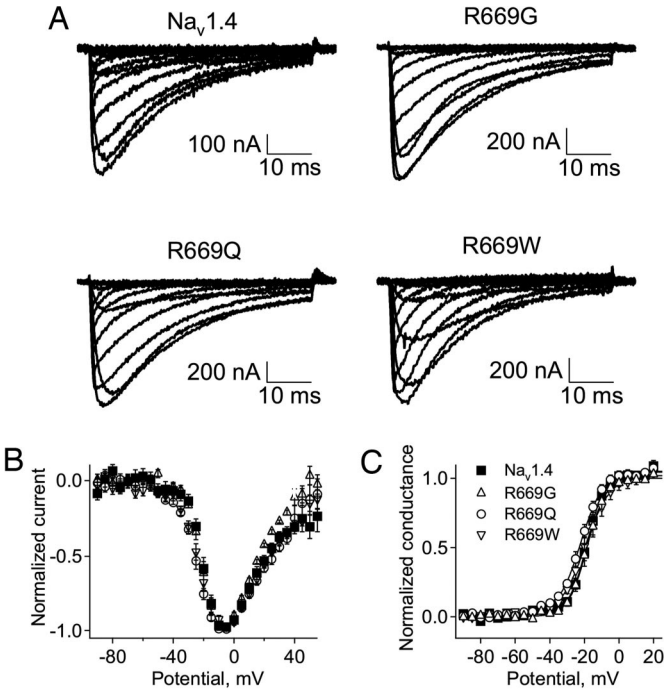

Fig. 1. Central pore Na^+ currents for WT $Na_v1.4$ and NormoPP mutants R669Q, R669G, and R669W. (*A*) Representative sodium currents through the central pore of the WT $Na_v1.4$, R669G, R669Q, and R669W channels in response to membrane depolarization from a holding potential of −100 mV to test potentials ranging from −90 to +50 mV in 10-mV increments. (*B*) Current–voltage relationships. (*C*) Conductance–voltage relationships. Normalized averages were not significantly different for $Na_v1.4$ (■, $V_{1/2} = -19 \pm 2$ mV, $n = 9$), R669G (△, $V_{1/2} = -18 \pm 2$ mV, $n = 6$), R669Q (○, $V_{1/2} = -22 \pm 2$ mV, $n = 11$), and R669W (▽, $V_{1/2} = -19 \pm 1$ mV, $n = 11$).

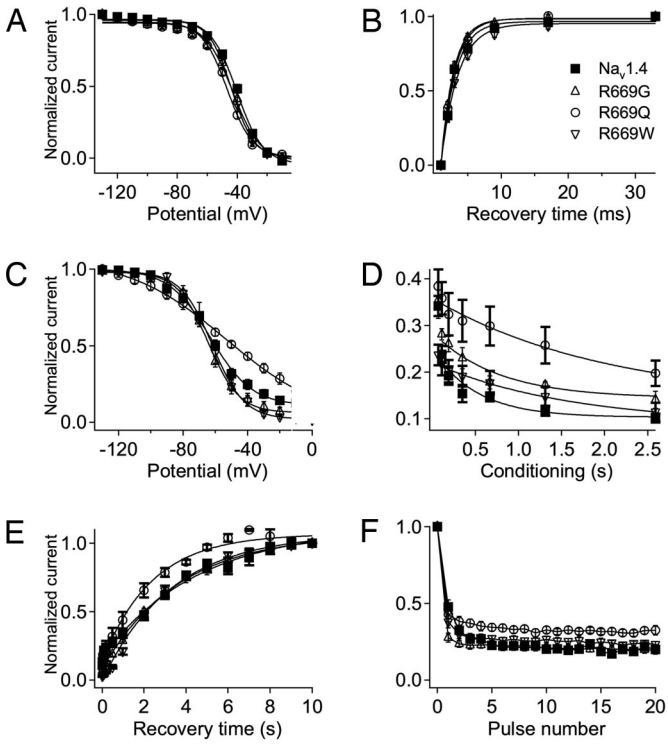

Fig. 2. Inactivation properties of NormoPP mutants R669Q, R669G, and R669W. (*A*) Steady-state fast inactivation in WT $Na_v1.4$ (■), R669Q (○), R669G (△), and R669W (▽) was measured after 200-ms conditioning pulses to voltages ranging from −130 to 10 mV in 10-mV increments. Normalized averages were fit with a Boltzmann equation with the following parameters: $Na_v1.4$, $V_{1/2} = -41 \pm 2$ mV, $k = 9 \pm 1$ mV, $n = 15$; R669Q, $V_{1/2} = -46 \pm 2$ mV, $k = 9 \pm 1$ mV, $n = 15$; R669G, $V_{1/2} = -43 \pm 1$ mV, $k = 9 \pm 1$ mV, $n = 11$; R669W, $V_{1/2} = -44 \pm 1$ mV, $k = 8 \pm 1$ mV, $n = 16$. (*B*) Kinetics of recovery from fast inactivation at −100 mV for: $Na_v1.4$, $\tau = 2.1 \pm 0.1$ ms, $n = 10$; R669Q, $\tau = 2.0 \pm 0.1$ s, $n = 14$; R669G, $\tau = 1.9 \pm 0.1$ s, $n = 9$; R669W, $\tau = 2.5 \pm 0.1$ s, $n = 15$. Fast inactivation was induced by 20-ms conditioning depolarization to −10 mV, and recovery was assessed by a 5-ms test pulse to −10 mV after the indicated recovery intervals. (*C*) Steady-state slow inactivation in WT $Na_v1.4$, R669Q, R669G, and R669W was induced by 30-s conditioning pulses to voltages ranging from −130 to 0 mV in 10-mV increments. A 5-ms test pulse to −10 mV was preceded by 20-ms repolarization to −130 mV to allow recovery from fast inactivation. Data were normalized and fit with a Boltzmann equation with the following parameters: $Na_v1.4$, $V_{1/2} = -63 \pm 1$ mV, $k = 13 \pm 1$ mV, $n = 6$; R669Q, $V_{1/2} = -53 \pm 2$ mV, $k = 30 \pm 2$, $n = 5$; R669G, $V_{1/2} = -64 \pm 1$ mV, $k = 9 \pm 1$ mV, $n = 10$; R669W, $V_{1/2} = -62 \pm 1$ mV, $k = 9 \pm 1$ mV, $n = 6$. (*D*) Kinetics of onset of slow inactivation during conditioning pulses to −10 mV of indicated durations was measured with a 5-ms test pulse to −10 mV preceded by 20 ms at −100 mV to allow recovery from fast inactivation. Data were fit with single exponential curves with the following parameters: $Na_v1.4$, $\tau = 0.5 \pm 0.1$ s, $n = 4$; R669Q, $\tau = 1.6 \pm 0.2$ s, $n = 4$; R669G, $\tau = 0.7 \pm 0.1$ s, $n = 4$; R669W, $\tau = 2.0 \pm 0.2$ s, $n = 7$. (*E*) Kinetics of recovery from slow inactivation at −100 mV for: $Na_v1.4$, $\tau = 4.5 \pm 0.3$ s, $n = 4$; R669Q, $\tau = 2.5 \pm 0.1$ s, $n = 6$; R669G, $\tau = 3.3 \pm 0.1$ s, $n = 4$; R669W, $\tau = 3.3 \pm 0.2$ s, $n = 6$. Slow inactivation was induced by 10-s conditioning depolarizations to −10 mV, and recovery was assessed by a train of 5-ms test pulses to −10 mV at the indicated time intervals. (*F*) Use-dependent accumulation of slow inactivation for $Na_v1.4$ ($n = 4$), R669Q ($n = 5$), R669G ($n = 4$), and R669W ($n = 5$) was estimated by a protocol that included a 40-ms conditioning depolarization to 0 mV to induce inactivation, a 20-ms repolarization to −100 mV allowing recovery from fast inactivation, and a 10-ms test pulse to 0 mV measuring the amount of slow inactivation. This sequence was repeated at 5 Hz.

Results

Physiological Properties of NormoPP Mutants. WT rat skeletal muscle $Na_v1.4$ channels and NormoPP mutants R669Q, R669G, and R669W (the rat orthologs of human R675Q/G/W) were transiently expressed in *Xenopus* oocytes with the $Na_V\beta_1$ subunit. Electrophysiological properties of central pore sodium currents were examined 2–3 days after mRNA injection by using the cut-open oocyte voltage clamp technique (22). Current–voltage relationships were recorded in 120 mM external Na^+ as charge carrier in a series of 50-ms depolarizations from a holding potential of −100 mV (Fig. 1*A*). The kinetics (Fig. 1*A*), current–voltage relationship (Fig. 1*B*), and voltage dependence of activation (Fig. 1*C*) for central pore Na^+ currents conducted by NormoPP mutant channels did not differ significantly from WT. The expression level of R669Q and R669G mutants was not significantly different from the WT Nav1.4, whereas the R669W mutant was usually expressed at substantially lower levels (data not shown).

It is well established that impaired fast and/or slow inactivation plays a key role in the pathophysiology of HyperPP and paramyotonia congenita (8). In contrast, we found that the kinetics of fast inactivation (Fig. 1*A*), the voltage dependence of fast inactivation (Fig. 2*A*), and the rate of recovery from fast inactivation (Fig. 2*B*) of the NormoPP mutants were indistinguishable from the WT channel. Slow inactivation properties were also examined (Fig. 2 *C–F*). Mutant R669Q had moderately impaired slow inactivation, including shallower voltage dependence (Fig. 2*C*), slower onset (Fig. 2*D*), faster recovery (Fig. 2*E*), and slightly, but significantly ($P < 0.05$), less slow inactivation during trains of depolarizations (Fig. 2*F*). However, the slow inactivation of the other two NormoPP mutants, R669G and R669W, did not differ significantly from WT $Na_v1.4$ (Fig. 2 *C–F*). Thus, we conclude that impaired slow inactivation of NormoPP mutant R669Q may contribute to abnormal ionic homeostasis in skeletal muscle fibers in patients carrying that mutation, but changes in the activation and inactivation properties of these central pore

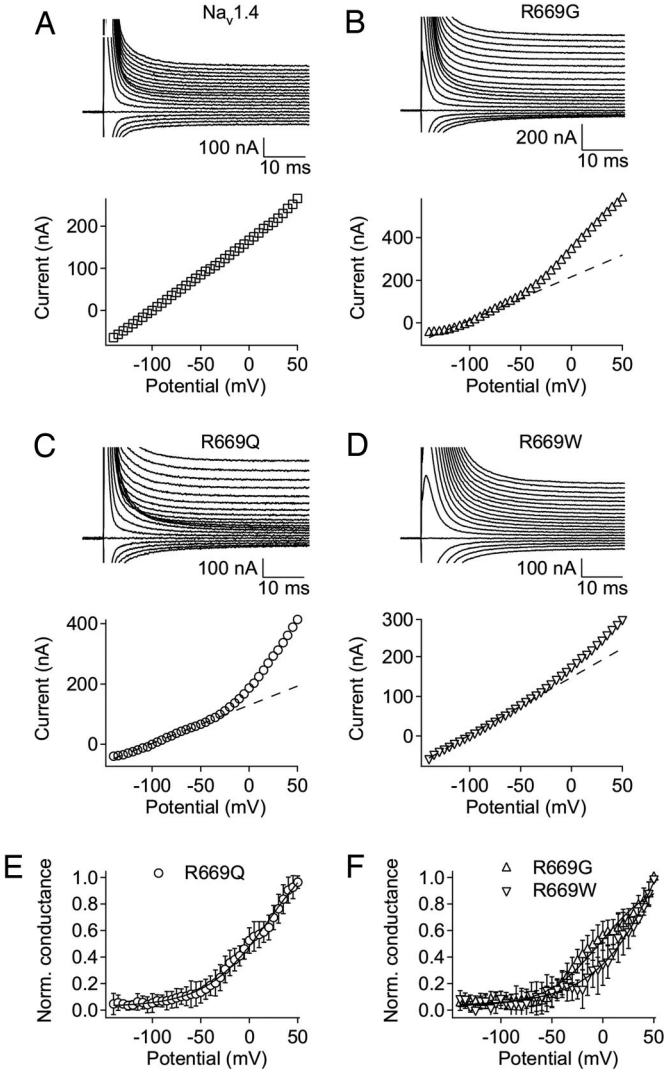

Fig. 3. Gating pore currents in NormoPP mutant channels. The central pore of Na$_V$1.4 channels was blocked by 1 μM TTX, and remaining currents through the oocyte membrane were measured in series of voltage steps from −140 to +50 mV in 5-mV increments (every second trace is shown) from the holding potential of −100 mV for Na$_v$1.4 (*A*), R669G (*B*), R669Q (*C*), and R669W (*D*). Dashed lines represent background linear leak in representative cells. (*E* and *F*) Normalized voltage dependence of gating pore conductance was calculated by differentiating current–voltage relationships. (*E*) R669Q, $n = 14$. (*F*) R669G (△, $n = 21$; R669W (▽), $n = 6$.

sodium currents alone cannot explain the pathophysiology of NormoPP patients because two of the three mutants did not have any impairment of these functions.

Gating Pore Current of NormoPP Mutants. Gating pore currents (13, 14, 21) [also called omega currents (23)] arise when gating-charge-carrying arginine residues in the S4 voltage sensors of sodium or potassium channels are mutated to small or hydrophilic amino acids, allowing cations to pass through the voltage sensor in the position of the positively charged arginine side chain (13, 14, 21, 23). To detect possible gating pore currents, we blocked the central pore of sodium channels with 1 μM tetrodotoxin (TTX) and recorded non-leak-subtracted currents in response to 50-ms voltage steps from a holding potential of −100 mV to a range of potentials from −140 mV to +50 mV. When the central pore of WT Na$_v$1.4 is blocked by TTX, the current–voltage relationship is linear over the full range studied (Fig. 3*A*), reflecting the background, voltage-independent leakage of ions through the oocyte membrane. In contrast, current–voltage plots of the non-leak-subtracted currents conducted by all three NormoPP mutants contained an additional nonlinear component at depolarized membrane potentials, revealing gating pore current through the mutant voltage sensors (Fig. 3 *B–D*). To illustrate the voltage dependence of this gating pore current more clearly, we estimated the gating pore conductance for each 5-mV voltage increment by calculating the local slope of the current–voltage relationship for that voltage interval (Fig. 3 *E* and *F*). These conductance–voltage plots show that gating pore conductance begins to increase at approximately −50 mV for all three mutants and continues to rise steeply up to +50 mV. This voltage-dependent increase in gating pore conductance begins at a similar voltage as activation of the central pore (Fig. 1*C*), but rises less steeply and continues to increase after the increase in central pore conductance has saturated.

Comparison of the Amplitudes of Gating Pore and Central Pore Conductance. Gating pore currents observed in R3 mutants are much smaller than central pore Na^+ current in the absence of TTX. Typically, expression of sodium channel protein to levels that cause poor voltage clamp control of the large central pore currents was required to achieve acceptable signal-to-noise ratio for gating pore current measurements. However, in favorable cases, we were able to estimate the central pore conductance in the absence of TTX, block the channels with TTX, and measure gating pore conductance in the same cell. In cells with central pore conductance reaching 150–250 μS, the gating pore conductance was 0.8–1.8 μS, corresponding to 0.8% ± 0.3% of the central pore conductance ($n = 4$).

Gating Pore Current Conducted by Slow-Inactivated NormoPP Channels. Under physiological conditions, activation of gating pore current in NormoPP mutants would only occur during the action potential. Because gating pore conductance is <1% of central pore conductance, it is difficult to envision an important pathophysiological role for this small gating pore current during the action potential. However, during trains of action potentials that generate forceful contractions in skeletal muscle, sodium channels progressively enter a slow-inactivated state, as illustrated for Na$_v$1.4 channels expressed in *Xenopus* oocytes in Fig. 2*F*. We therefore examined whether slow-inactivated NormoPP channels can conduct gating pore current.

To address this question, we compared the voltage dependence of gating pore conductance of mutant R669G at different holding potentials in the presence of TTX (Fig. 4*A*). First, gating pore current was measured in a series of depolarizing steps to test potentials from −140 mV to +50 mV, applied from a holding potential of −140 mV where all of the channels would be in the resting state. Second, after a 30-s depolarization to 0 mV to force most sodium channels into the slow-inactivated state (>90%; see Fig. 2*F*), gating pore current was measured in a series of hyperpolarizing steps from +50 mV to −140 mV. Finally, after 30 s at −140 mV to recover from slow inactivation, gating pore current was again recorded during a series of depolarizing steps from −140 mV to +50 mV from the holding potential of −140 mV. Gating pore current during the first series of 50-ms steps from holding potential of −140 mV increased with similar voltage dependence as observed in previous experiments (Fig. 4*A*, left black traces), yielding a conductance–voltage relationship that began to rise at −50 mV and continued to increase up to +50 mV (Fig. 4*B*, black symbols). Remarkably, after a 30-s depolarization to 0 mV to drive >90% of the sodium channels into the slow-inactivated state, the gating pore conductance at +50 mV was indistinguishable from that recorded for sodium channels in the activated state (Fig. 4*B*; R669G, red symbols, $P >$

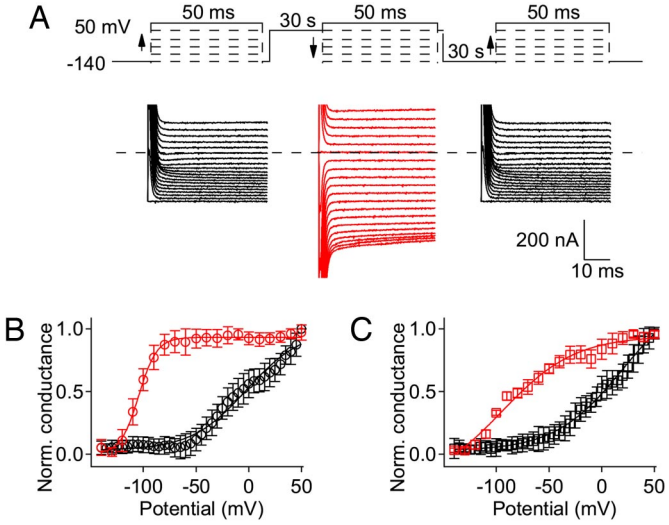

Fig. 4. Gating pore current in slow-inactivated NormoPP mutant channels. (*A*) Representative experiment demonstrating voltage dependence of gating pore current in R669G with and without slow inactivation. (*Left*) Gating pore current was first measured in a series of 50-ms steps from a holding potential of −140 mV in 5-mV increments (black). After this series, cells were held for 30 s at 0 mV to induce slow inactivation. (*Center*) The second series of 50-ms test pulses (red traces) were applied from holding potential of 0 mV in descending order from +50 mV in 10-mV decrements. (*Right*) After the second series, the holding potential was returned to −140 mV and channels were allowed to recover for 30 s before applying the last series of 50-ms test pulses (black traces), with protocol identical to the first series. (*B*) Voltage dependence of gating pore conductance for R669G with holding potentials of −140 mV (black symbols) and 0 mV (red symbols). Conductance was obtained by differentiation of steady-state currents measured at the end of 50-ms test pulses at each potential. Data were normalized after subtraction of background conductance in each cell measured at −140 mV and averaged ($n = 21$). (*C*) Results of a similar experiment for R669Q, $n = 15$.

0.1). This level of gating pore conductance remained nearly constant during progressively more negative test pulses down to −90 mV and then declined to the baseline at −140 mV (Fig. 4*B*, red symbols). Repeating the series of depolarizing pulses from the holding potential of −140 mV (Fig. 4*A Right*) gave the same depolarization-dependent increase in gating pore conductance observed in the initial series of depolarizing pulses (data not shown).

Similar results were observed for R669Q (Fig. 4*C*). The gating pore conductance began to increase at −50 mV, continued to increase up to +50 mV during the series of depolarizing pulses (Fig. 4*C*, black traces), and it remained high in the slow-inactivated state of R669Q at +50 mV (Fig. 4*C*, red traces). The gating pore conductance of R669Q began to decline to baseline at more positive potentials than for R669G, and significant deactivation was observed at −30 mV for R669Q compared with −90 mV for R669G (Fig. 4 *B* and *C*, red traces). Nevertheless, a substantial gating pore conductance of R669Q remained at potentials in the range of −80 to −90 mV, near the resting membrane potential of skeletal muscle fibers (Fig. 4*C*, red traces). The low level of expression made it difficult to carry out the same type of experiment for NormoPP mutant R669W accurately, but in the highest-expressing cells we also observed gating pore current in slow-inactivated channels for this mutant with voltage dependence of activation and deactivation similar to R669Q (data not shown). Together, these results show that slow-inactivated NormoPP channels would conduct substantial gating pore current at the resting membrane potential and both during and after trains of action potentials in skeletal muscle fibers, and therefore would produce a substantial increase in total sodium influx and a sustained depolarization.

The voltage dependence of deactivation of the gating pore conductance during a series of hyperpolarizing pulses is shifted to far more negative membrane potentials than the voltage dependence of activation of the gating pore conductance during a series of depolarizing pulses (Fig. 4 *B* and *C*). Such hysteresis is expected from previous work on the effects of slow inactivation on gating charge movement (24). After activation of the voltage sensors and induction of slow inactivation, repolarization to very negative membrane potentials is required for recovery of gating charge movement and return to the resting state of the voltage sensors (25, 26). Evidently, the gating charges in the voltage sensor must be driven back to their resting conformation at hyperpolarized voltages to allow closure of the gating pore in mutant NormoPP channels.

Discussion

NormoPP Mutants Conduct Gating Pore Current in the Activated and Slow-Inactivated States. Our results show that NormoPP mutants conduct substantial gating pore currents, in the range of 0.8% of the peak central pore current. In contrast to HypoPP mutants, the gating pores in NormoPP mutants are open in the activated state of the voltage sensor. This voltage dependence was predicted from our previous work on site-directed mutations in the voltage sensor of brain sodium channels (21). This finding is consistent with recent experiments in which disulfide cross-linking was used to track the movement of the R3 gating charge during channel activation (27). Those results showed that activation of the voltage sensor moves the R3 gating charge of the bacterial sodium channel NaChBac into position to form a disulfide bond with residue D60, located in the S2 segment near the extracellular limit of the narrow part of the gating pore (28–30). Evidently, when R3 is neutralized by mutation to G, Q, or W in $Na_V1.4$, monovalent cations can move inward through the gating pore. The ability of the voltage sensor to conduct gating pore current in the resting and activated states in both site-directed (21) and naturally occurring (refs. 13 and 14 and this work) mutants indicates that the S4 segment is in a transmembrane position in both resting and activated states, consistent with the sliding helix model of gating (30–33) but not with the paddle model of gating (34).

Gating pore current is conducted by the voltage sensor of NormoPP mutants in the slow-inactivated state in addition to the activated state. Surprisingly, slow inactivation did not significantly change the amplitude of the gating pore current recorded at +50 mV, indicating that conductance of gating pore in the activated and slow-inactivated states of the voltage sensor is comparable. These results suggest that the voltage sensor is in a similar conformation in the activated and slow-inactivated states because the gating pore conductance is expected to be very sensitive to small changes in the locations of amino acid residues in the gating pore. Similarly, because gating pore current is constant during long depolarizations that cause fast inactivation followed by slow inactivation, the voltage sensor is also likely to remain in a similar conformation during both fast and slow inactivation. Therefore, we hypothesize that the IIS4 segment moves outward upon depolarization, following a spiral path and exchanging ion pair partners according to the sliding helix model (30–33), until gating charge R3 enters the narrow segment of the gating pore. In this conformation of the voltage sensor, the central pore opens, both fast and slow inactivation processes are engaged in WT and NormoPP mutants, and gating pore current is conducted when the R3 gating charge is mutated in NormoPP or by site-directed mutations.

Our experiments on deactivation of the gating pore current conducted by slow-inactivated NormoPP channels (Fig. 4 *B* and *C*, red symbols) also demonstrate immobilization of the IIS4

voltage sensor during slow inactivation, as previously inferred for the entire sodium channel from gating current measurements (25, 26, 35). The large negative shift of deactivation of the gating pore current conducted by the slow-inactivated NormoPP channels implies that slow inactivation greatly stabilizes the IIS4 voltage sensor in its activated conformation and resists return of the voltage sensor to its resting state. Evidently, the movement of the IIS4 voltage sensor is tightly coupled to the slow inactivation process.

Role of Gating Pore Current in the Pathophysiology of NormoPP. Gating pore current is thought to be the primary cause of pathophysiology in HypoPP (13, 14, 36, 37). In the HypoPP mutants, neutralization of the R1 or R2 gating charges produces gating pore current in the resting state. For the mutation R666G, sodium conductance through the gating pore in the resting state would directly increase the resting sodium influx into the muscle fiber, depolarize it because of the increase in resting sodium current and the sodium overload, and thereby impair action potential generation by both the mutant and WT alleles of $Na_V1.4$ channels (13). For the HypoPP mutations R666H and R669H, the primary permeant ion is protons, but these mutations are proposed to increase sodium influx and produce sodium overload indirectly by hyperactivation of sodium–proton exchange (14). Thus, sodium overload is thought to be the common element in the pathophysiology of HypoPP.

The NormoPP mutants described here would also increase sodium entry into the muscle fiber because of the gating pore conductance in the activated and slow-inactivated states of the channel. Although gating pore current that we have measured in the range of -50 to $+50$ mV is an outward current carried primarily by intracellular potassium, the inward gating pore current conducted by slow-inactivated NormoPP mutant $Na_V1.4$ channels after repolarization to membrane potentials near the equilibrium potential for potassium is carried primarily by extracellular sodium. Changes in extracellular proton concentration of >100-fold (pH 5.6 to 8.3) had no effect on either inward or outward gating pore current, eliminating protons as a major permeant ion for these NormoPP mutants (data not shown). Although gating pore conductance would contribute little to sodium influx during the action potential, compared with the large sodium influx through the open central pore, it is estimated that 45% of skeletal muscle sodium channels in fast-twitch fibers and 17% in slow-twitch fibers reside in slow-inactivated state at the resting membrane potential (38). In addition, the number of sodium channels in the slow-inactivated state increases during and after trains of action potentials that are elicited by tetanic stimulation by the motor nerves during forceful contractions. Therefore, at the resting membrane potential and during the repolarization phase within and after trains of action potentials, sodium would be the primary cation entering the cell through the gating pore, and gating pore current through the slow-inactivated voltage sensor in domain II of the NormoPP mutants would lead to abnormal persistent sodium influx. This sodium influx would depolarize the muscle fiber, increase intracellular sodium, impair action potential generation, and cause cellular pathology of NormoPP muscle fibers, similar to the postulated role of sodium overload in the pathophysiology of HypoPP (13, 14).

We estimated previously that the HypoPP mutation R666G increases resting sodium influx into human muscle fibers by 21-fold (13). The increase in resting sodium influx for NormoPP mutations would be much less, in the range of 9.4-fold for fast-twitch fibers and 3.6-fold for slow-twitch fibers, because only 45% of sodium channels in fast-twitch human muscle fibers and 17% of sodium channels in slow-twitch human muscle fibers are in the slow-inactivated state at rest. However, most sodium channels enter the slow-inactivated state at the end of long trains of action potentials (e.g., Fig. 2*F*), as occur during forceful muscle contractions, so it is likely that resting sodium influx between action potentials and after trains of action potentials in fast-twitch fibers is increased substantially >10-fold. In addition, the NormoPP mutations would cause a positive feedback loop in which sodium influx via the gating pore would depolarize muscle fibers and cause more slow inactivation, which would in turn cause more gating pore current. It is likely that the combination of the large increase in sodium influx between action potentials and after trains of action potentials with the positive feedback loop to increase slow inactivation and sodium influx is sufficient to generate substantial sodium overload and cause the symptoms of NormoPP.

In the case of HypoPP, we hypothesized that the ability of low-serum potassium to precipitate attacks of weakness may result from the reduction in activity of the Na,K-ATPase caused by reduced extracellular potassium (13). Reduced extracellular potassium would also hyperpolarize skeletal muscle fibers, driving more sodium channels into the resting state that conducts gating pore current in HypoPP. These two effects would work in concert to produce gating pore current. In contrast, in NormoPP, these two effects of reduced extracellular potassium would oppose each other. The activity of the Na,K-ATPase would be slowed, impairing sodium pumping, but hyperpolarization would drive more sodium channels into the resting state, reducing gating pore current through the gating pore of NormoPP mutants. This balance of effects may prevent precipitation of attacks of weakness by low serum potassium in NormoPP. Thus, as for HypoPP, gating pore current conducted by NormoPP mutants can potentially cause all of the aspects of the pathophysiology of the disease.

Materials and Methods

Site-Directed Mutagenesis. cDNA encoding rat $Na_v1.4$ α-subunit (2, 39) subcloned into the pCDM8 vector (40) was used as a template for PCR-based site-directed mutagenesis as described (41).

Expression in *Xenopus* Oocytes. Isolation, preparation, and maintenance of *Xenopus* oocytes were carried out as described (41). RNA transcription was performed with T7 RNA polymerase (Ambion). Healthy stage V–VI oocytes selected manually were pressure-injected with 50 nL of a solution containing a 1:1 molar ratio of α- to β1-subunit RNA. Electrophysiological recordings were carried out 2–10 days after injection.

Cut-Open Oocyte Voltage Clamp. Cut-open oocyte voltage-clamp experiments were performed as described by Stefani and Bezanilla (22), and access to the cytoplasm was obtained by rupturing the vegetal pole membrane of the oocyte as described (13). P/-4 leak subtraction from a holding potential of -100 mV was used for central pore current experiments in Figs. 1 and 2. The background leak component was subtracted offline for gating pore current experiments in Figs. 3 and 4. For experiments at a holding potential of -100 mV (Figs. 1–3), extracellular solution contained 120 mM Na^+-methanesulfonate, 1.8 mM Ca-methanesulfonate, and 10 mM Hepes, pH 7.4. For experiments at -140 mV holding potential (Fig. 4), the external solution contained 115 mM Na-methanesulfonate, 1.5 mM Ca-methanesulfonate, 2.5 mM Ba-methanesulfonate, and 10 mM Hepes, pH 7.4. Intracellular solution in all cases consisted of 110 mM K-methanesulfonate, 10 mM Na-methanesulfonate, 10 mM EGTA, and 10 mM Hepes, pH 7.4. In gating pore current experiments, sodium currents through the central pore were blocked by addition of 1 μM TTX to all solutions. Oocytes were preconditioned in TTX-containing solutions for 15–30 min. Experiments where central pore and gating pore currents were measured in the same cell were performed by first measuring central pore currents in TTX-free external solution, adding 38 μL of 5 μM TTX to block the central pore, and recording gating pore currents. Voltage-clamp protocols are described in the figure legends. Pooled data are reported as means ± SE. Statistical comparisons were done by using Student's *t* test, with $P < 0.05$ as the criterion for significance.

ACKNOWLEDGMENTS. This research was supported by research grants from the Muscular Dystrophy Association and the National Institutes of Health (Grant R01 NS15751, to W.A.C.).

1. Barchi RL (1983) Protein components of the purified sodium channel from rat skeletal sarcolemma. *J Neurochem* 36:1377–1385.
2. Trimmer JS, *et al.* (1989) Primary structure and functional expression of a mammalian skeletal muscle sodium channel. *Neuron* 3:33–49.
3. Isom LL, *et al.* (1992) Primary structure and functional expression of the β1 subunit of the rat brain sodium channel. *Science* 256:839–842.
4. Catterall WA (2000) From ionic currents to molecular mechanisms: The structure and function of voltage-gated sodium channels. *Neuron* 26:13–25.
5. Yu FH, Yarov-Yarovoy V, Gutman GA, Catterall WA (2005) Overview of molecular relationships in the voltage-gated ion channel superfamily. *Pharmacol Rev* 57:387–395.
6. Bezanilla F (2000) The voltage sensor in voltage-dependent ion channels. *Physiol Rev* 80:555–592.
7. Venance SL, *et al.* (2006) The primary periodic paralyses: Diagnosis, pathogenesis, and treatment. *Brain* 129:8–17.
8. Cannon SC (2006) Pathomechanisms in channelopathies of skeletal muscle and brain. *Annu Rev Neurosci* 29:387–415.
9. Struyk AF, Scoggan KA, Bulman DE, Cannon SC (2000) The human skeletal muscle Na channel mutation R669H associated with hypokalemic periodic paralysis enhances slow inactivation. *J Neurosci* 20:8610–8617.
10. Jurkat-Rott K, *et al.* (2000) Voltage-sensor sodium channel mutations cause hypokalemic periodic paralysis type 2 by enhanced inactivation and reduced current. *Proc Natl Acad Sci USA* 97:9549–9554.
11. Bendahhou S, Cummins TR, Griggs RC, Fu YH, Ptacek LJ (2001) Sodium channel inactivation defects are associated with acetazolamide-exacerbated hypokalemic periodic paralysis. *Ann Neurol* 50:417–420.
12. Kuzmenkin A, *et al.* (2002) Enhanced inactivation and pH sensitivity of Na^+ channel mutations causing hypokalaemic periodic paralysis type II. *Brain* 125:835–843.
13. Sokolov S, Scheuer T, Catterall WA (2007) Gating pore current in an inherited ion channelopathy. *Nature* 446:76–78.
14. Struyk AF, Cannon SC (2007) A Na^+ channel mutation linked to hypokalemic periodic paralysis exposes a proton-selective gating pore. *J Gen Physiol* 130:11–20.
15. Poskanzer DC, Kerr DN (1961) A third type of periodic paralysis, with normokalemia and favorable response to sodium chloride. *Am J Med* 31:328–342.
16. Meyers KR, Gilden DH, Rinaldi CF, Hansen JL (1972) Periodic muscle weakness, normokalemia, and tubular aggregates. *Neurology* 22:269–279.
17. Danowski TS, *et al.* (1975) Clinical and ultrastructural observations in a kindred with normo-hyperkalaemic periodic paralysis. *J Med Genet* 12:20–28.
18. Plassart E, *et al.* (1994) Mutations in the muscle sodium channel gene (SCN4A) in 13 French families with hyperkalemic periodic paralysis and paramyotonia congenita: Phenotype to genotype correlations and demonstration of the predominance of two mutations. *Eur J Hum Genet* 2:110–124.
19. Chinnery PF, Walls TJ, Hanna MG, Bates D, Fawcett PR (2002) Normokalemic periodic paralysis revisited: Does it exist? *Ann Neurol* 52:251–252.
20. Vicart S, *et al.* (2004) New mutations of SCN4A cause a potassium-sensitive normokalemic periodic paralysis. *Neurology* 63:2120–2127.
21. Sokolov S, Scheuer T, Catterall WA (2005) Ion permeation through a voltage- sensitive gating pore in brain sodium channels having voltage sensor mutations. *Neuron* 47:183–189.
22. Stefani E, Bezanilla F (1998) Cut-open oocyte voltage-clamp technique. *Methods Enzymol* 293:300–318.
23. Tombola F, Pathak MM, Isacoff EY (2005) Voltage-sensing arginines in a potassium channel permeate and occlude cation-selective pores. *Neuron* 45:379–388.
24. Bezanilla F, Perozo E, Papaziam DM, Stefani E (1991) Molecular basis of gating charge immobilization in Shaker potassium channels. *Science* 254:679–683.
25. Bezanilla F, Tailor RE, Fernandez JM (1982) Distribution and kinetics of membrane dielectric polarization. 1. Long-term inactivation of gating currents. *J Gen Physiol* 79:21–40.
26. Kuzmenkin A, Bezanilla F, Correa AM (2004) Gating of the bacterial sodium channel, NaChBac: Voltage-dependent charge movement and gating currents. *J Gen Physiol* 124:349–356.
27. DeCaen P, Yarov-Yarovoy V, Zhao Y, Scheuer T, Catterall WA (2008) Disulfide locking a sodium channel voltage sensor reveals ion pair formation during activation. *Proc Natl Acad Sci USA* 105:15142–15147.
28. Long SB, Campbell EB, MacKinnon R (2005) Voltage sensor of $K_v1.2$: structural basis of electromechanical coupling. *Science* 309:903–908.
29. Long SB, Tao X, Campbell EB, MacKinnon R (2007) Atomic structure of a voltage-dependent K^+ channel in a lipid membrane-like environment. *Nature* 450:376–382.
30. Yarov-Yarovoy V, Baker D, Catterall WA (2006) Voltage sensor conformations in the open and closed states in ROSETTA structural models of K^+ channels. *Proc Natl Acad Sci USA* 103:7292–7297.
31. Catterall WA (1986) Molecular properties of voltage-sensitive sodium channels. *Annu Rev Biochem* 55:953–985.
32. Guy HR, Seetharamulu P (1986) Molecular model of the action potential sodium channel. *Proc Natl Acad Sci USA* 83:508–512.
33. Shafrir Y, Durell SR, Guy HR (2008) Models of the structure and gating mechanisms of the pore domain of the NaChBac ion channel. *Biophys J* 95:3650–3662.
34. Jiang Y, Ruta V, Chen J, Lee A, MacKinnon R (2003) The principle of gating charge movement in a voltage-dependent K^+ channel. *Nature* 423:42–48.
35. Cha A, Ruben PC, George AL, Jr, Fujimoto E, Bezanilla F (1999) Voltage sensors in domains III and IV, but not I and II, are immobilized by Na^+ channel fast inactivation. *Neuron* 22:73–87.
36. Jurkat-Rott K, Lehmann-Horn F (2007) Do hyperpolarization-induced proton currents contribute to the pathogenesis of hypokalemic periodic paralysis, a voltage sensor channelopathy? *J Gen Physiol* 130:1–5.
37. Struyk AF, Cannon SC (2008) Paradoxical depolarization of Ba^{2+}-treated muscle exposed to low extracellular K^+: Insights into resting potential abnormalities in hypokalemic paralysis. *Muscle Nerve* 37:326–337.
38. Ruff RL (1996) Sodium channel slow inactivation and the distribution of sodium channels on skeletal muscle fibers enable the performance properties of different skeletal muscle fibre types. *Acta Physiol Scand* 156:159–168.
39. Featherstone DE, Fujimoto E, Ruben PC (1998) A defect in skeletal muscle sodium channel deactivation exacerbates hyperexcitability in human paramyotonia congenita. *J Physiol (London)* 506:627–638.
40. Yu FH, *et al.* (2003) Sodium channel beta4, a new disulfide-linked auxiliary subunit with similarity to β2. *J Neurosci* 23:7577–7585.
41. McPhee JC, Ragsdale DS, Scheuer T, Catterall WA (1995) A critical role for transmembrane segment IVS6 of the sodium channel α subunit in fast inactivation. *J Biol Chem* 270:12025–12034.